

# Nonlinear effects on charge fractionalization in critical chains

Flávia B. Ramos,<sup>1</sup> Rodrigo G. Pereira,<sup>2</sup> Sebastian Eggert,<sup>1</sup> and Imke Schneider<sup>1</sup>

<sup>1</sup>*Physics Department and Research Center OPTIMAS,*

*University of Kaiserslautern-Landau, 67663 Kaiserslautern, Germany*

<sup>2</sup>*International Institute of Physics and Departamento de Física Teórica e Experimental,*  
*Universidade Federal do Rio Grande do Norte, Natal, RN, 59078-970, Brazil*

(Dated: June 10, 2024)

We investigate the generic transport in a one-dimensional strongly correlated fermionic chain beyond linear response. Starting from a Gaussian wave packet with positive momentum on top of the ground state, we find that the numerical time evolution splits the signal into at least three distinct fractional charges moving with different velocities. A fractional left-moving charge is expected from conventional Luttinger liquid theory, but for the prediction of the two separate right-moving packets the nonlinearity of the dispersion must also be taken into account. This out-of-equilibrium protocol therefore allows a direct measurement of nonlinear interaction parameters, which also govern threshold singularities of dynamic response functions. The nonlinear Luttinger Liquid theory also predicts the correct dynamics at low energies, where it agrees with the conventional Luttinger liquid. Moreover, at high energies, the wave packet dynamics reveals signatures of composite excitations containing two-particle bound states. Our results uncover a simple strategy to probe the nonlinear regime in time-resolved experiments in quantum wires and ultracold-atom platforms.

*Introduction.*— The fractionalization of a particle into a composite of emergent excitations is one of the most striking phenomena in quantum many-body systems. The effect is prevalent in critical one-dimensional (1D) systems, in which interactions inevitably lead to a departure from Fermi liquid behavior [1–3]. Within the paradigm of Luttinger liquid (LL) theory [4, 5], the low-energy spectrum of 1D quantum fluids is described by bosonic collective modes with a linear dispersion relation. This theory predicts that electrons fractionalize into right- and left-moving excitations that carry interaction-dependent charges [6, 7], as indeed observed in transport experiments in quantum wires [8–11]. In addition, signatures of LL behavior have been identified via spectroscopic techniques [12–17] and quantum simulations in ultracold-atom platforms [18–21].

Despite its impressive success, LL theory breaks down whenever finite-energy excitations and band curvature have to be taken into account [22]. To treat the effects of a nonlinear dispersion, more general techniques have been developed into what became known as the nonlinear Luttinger liquid (nLL) theory [23–27]. In particular, dynamic response functions exhibit characteristic threshold singularities that can be described by treating the modes with finite energy and momentum as mobile impurities coupled to the gapless modes [24]. The exponents associated with these singularities can be expressed in terms of scattering phase shifts and calculated exactly for integrable models [27–30]. In the time domain, the contributions from high-energy modes give rise to power-law-decaying temporal oscillations that dominate the long-time behavior [31]. Moreover, nonlinearities are predicted to lead to shock waves in the evolution of density and magnetization pulses [32–35].

While the nonlinear regime is accessible in experiments

[36–39], direct tests of the threshold singularities predicted by nLL theory are hindered by the limited energy resolution or disorder-induced broadening of spectroscopic probes. In this work, we show that the effects of the high-energy excitation in nLL theory can be directly observed in an out-of-equilibrium protocol. We create a Gaussian wave packet with preselected momentum in a critical fermionic chain and simulate its evolution using the adaptive time-dependent density matrix renormalization group (tDMRG) [40]. Similar protocols have been used to demonstrate fractionalization and spin-charge separation in the low-energy regime [41–47]. Beyond the LL paradigm, the nonlinear dispersion leads to a splitting of the initial wave packet into three density humps that propagate with different velocities [48, 49]. Here, we show that the time-evolved signal can be predicted by nLL theory, which in turn provides a quantitative measurement of the interaction between the high-energy particle and the low-energy modes. At lower fillings and higher energies, we discover fingerprints of two-particle bound states in the wave packet dynamics.

*Model and protocol.*— We consider a spinless fermion model described by the Hamiltonian

$$H = \sum_{j=1}^L \left[ -\frac{1}{2} (c_j^\dagger c_{j+1} + \text{h.c.}) + V n_j n_{j+1} \right], \quad (1)$$

where  $c_j$  annihilates a fermion at site  $j$  of a chain with  $L$  sites,  $V$  is the strength of the nearest-neighbor interaction, and  $n_j = c_j^\dagger c_j$  is the local density operator. We work at fixed number of fermions  $N$ , with average density  $n = N/L$ . For  $V = 0$ , the Hamiltonian can be diagonalized as  $H_0 = \sum_k \varepsilon_0(k) c_k^\dagger c_k$ , where  $\varepsilon_0(k) = -\cos(k)$  is the dispersion relation of free fermions with momentum  $k \in [-\pi, \pi]$ , with lattice spacing set to unity. The ground state in this case is constructed by occupying single-

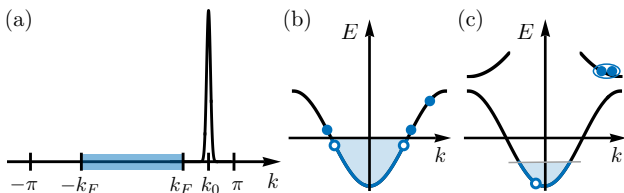


FIG. 1. (a) Gaussian wave packet in momentum space. (b) At half filling, the evolution is controlled by a particle above the Fermi level and low-energy particle-hole excitations. (c) At lower fillings, there are contributions from excitations with a hole and two particles in a high-energy bound-state band.

particle states up to the Fermi momentum  $k_F = \pi n$ . More generally, the model in Eq. (1) is equivalent to the spin-1/2 XXZ chain and is exactly solvable via Bethe ansatz (BA) [50]. We focus on the parameter regime  $0 \leq V \leq 1$ , where the ground state  $|\Psi_0\rangle$  of Eq. (1) is in a gapless phase described at low energies by LL theory [1].

We prepare an initial state given by

$$|\Psi(t=0)\rangle = A \sum_{j=1}^L e^{-\frac{(j-j_0)^2}{2\sigma_0^2}} e^{ik_0 j} c_j^\dagger |\Psi_0\rangle, \quad (2)$$

corresponding to a Gaussian wave packet centered at  $j_0$ , with variance  $\sigma_0^2/2$  in real space and mean momentum  $k_0$ ; here,  $A$  is a normalization constant. To add a particle with well-defined momentum, we choose  $k_0 \in [k_F, \pi]$  with momentum uncertainty  $\Delta k = \frac{1}{\sqrt{2\sigma_0^2}}$ ; see Fig. 1(a). After the unitary evolution  $|\Psi(t)\rangle = e^{-iHt} |\Psi(0)\rangle$ , we measure the time-dependent local charge excess defined as

$$\rho_j(t) = \langle \Psi(t) | n_j | \Psi(t) \rangle - \langle \Psi_0 | n_j | \Psi_0 \rangle. \quad (3)$$

*Free fermions.*— The local charge excess can be calculated exactly in the noninteracting case. For a finite chain with open boundary conditions, we obtain

$$\rho_j(t) = \left| \sum_{l=N+1}^L q(k_l) \sin(k_l j) e^{i \cos(k_l) t} \right|^2, \quad (4)$$

where  $q(k) = \frac{2A}{L+1} \sum_{j=1}^L e^{-\frac{(j-j_0)^2}{2\sigma_0^2}} e^{ik_0 j} \sin(kj)$  and  $k_l = \frac{l\pi}{L+1}$  with  $l = 1, \dots, L$ . The result is analogous to the evolution of a Gaussian wave packet in the single-particle problem [51]. For small  $\Delta k$ , we can expand the dispersion as  $\varepsilon_0(k) \approx \varepsilon_0(k_0) + u_0(k - k_0) + \frac{1}{2m_0}(k - k_0)^2$ , where  $u_0 = \sin(k_0)$  is the group velocity and  $m_0 = [\cos(k_0)]^{-1}$  is the effective mass for momentum  $k_0$ . As a consequence, we observe a single packet that moves to the right with velocity  $u_0$  and width growing as

$$\sigma(t)^2 \approx \sigma_0^2 \left( 1 + \frac{t^2}{m_0^2 \sigma_0^4} \right). \quad (5)$$

We have used Eq. (4) to benchmark our tDMRG results, obtaining excellent agreement; see the Supplemental Material (SM) [52]. In all the numerics henceforth, we set  $L = 300$ ,  $j_0 = 150$ , and  $\sigma_0 = 14.5$ . We keep up to 400 states per DMRG block and use the Trotter step  $\delta t = 0.1$ . The largest truncation error is of order  $10^{-10}$ . The maximum time is set by stopping the simulations before the wave packets reach the chain boundaries.

*nLL theory.*— We now turn to the interacting case. We seek to describe the dynamics using the framework of nLL theory [22]. In addition to the momentum  $k_0$ , we consider a mode expansion that includes the low-energy modes in the vicinity of the Fermi points [see Fig. 1(b)]:

$$c_j^\dagger \sim e^{-ik_F x} \psi_R^\dagger(x) + e^{ik_F x} \psi_L^\dagger(x) + e^{-ik_0 x} d^\dagger(x). \quad (6)$$

In the absence of the high-energy particle created by  $d^\dagger$ , the low-energy modes are described by the LL Hamiltonian [1]

$$H_{LL} = \frac{v}{2} \int dx \left[ (\partial_x \varphi_R)^2 + (\partial_x \varphi_L)^2 \right], \quad (7)$$

where  $v$  is the velocity of the low-energy modes and  $\varphi_{R,L}(x)$  are the right- and left-moving components of the bosonic field obeying

$$[\partial_x \varphi_{R,L}(x), \varphi_{R,L}(x')] = \pm i \delta(x - x'). \quad (8)$$

The low-energy fermion fields can be bosonized in the form

$$\psi_{R,L}^\dagger(x) \sim e^{i\sqrt{\frac{\pi}{2K}}[(1\pm K)\varphi_R(x) + (1\mp K)\varphi_L(x)]}, \quad (9)$$

where  $K$  is the Luttinger parameter. Taking the continuum limit of Eq. (1) including the high-energy mode, we obtain the effective Hamiltonian

$$H_{nLL} = H_{LL} + \int dx d^\dagger (\varepsilon_p - iu\partial_x) d + \frac{1}{\sqrt{2\pi K}} \int dx (\kappa_R \partial_x \varphi_R + \kappa_L \partial_x \varphi_L) d^\dagger d, \quad (10)$$

where  $\varepsilon_p$  and  $u$  are the renormalized energy and velocity, respectively, of the high-energy particle in the interacting model. Note that the high-energy particle behaves as a mobile impurity [53, 54] that interacts with the bosonic modes via the coupling constants  $\kappa_{R,L}$ .

The impurity mode can be decoupled from the bosonic fields by the unitary transformation  $U = e^{-i \int \frac{dx}{\sqrt{2\pi K}} (\gamma_R \varphi_R + \gamma_L \varphi_L) d^\dagger d}$ , where  $\gamma_{R,L} = \kappa_{R,L}/(v \mp u)$  are the right- and left-mover phase shifts. In the nLL,  $\gamma_{R,L}$  govern all the space-time correlation functions of the system as well as the threshold singularities of dynamic response functions [24, 27]. As we will see below, these non-trivial interaction parameters can be measured as fractional charges in our proposed out-of-equilibrium protocol.

We now proceed to calculate the fractional transport properties using the nLL theory. Up to irrelevant terms, the transformed Hamiltonian  $\tilde{H}_{\text{nLL}} = U H_{\text{nLL}} U^\dagger$  becomes noninteracting [55]

$$\tilde{H}_{\text{nLL}} = \frac{v}{2} \left[ (\partial_x \tilde{\varphi}_R)^2 + (\partial_x \tilde{\varphi}_L)^2 \right] + \tilde{d}^\dagger (\varepsilon_p - iu \partial_x) \tilde{d}, \quad (11)$$

with

$$\partial_x \varphi_{R,L} = U^\dagger \partial_x \tilde{\varphi}_{R,L} U = \partial_x \tilde{\varphi}_{R,L} \pm \frac{\gamma_{R,L}}{\sqrt{2\pi K}} \tilde{d}^\dagger \tilde{d}, \quad (12)$$

$$\tilde{d}^\dagger = U^\dagger \tilde{d}^\dagger U = \tilde{d}^\dagger e^{\frac{i}{\sqrt{2\pi K}} \gamma_R \tilde{\varphi}_R} e^{\frac{i}{\sqrt{2\pi K}} \gamma_L \tilde{\varphi}_L}. \quad (13)$$

Note that an initial excitation  $\tilde{d}^\dagger$  now consists of three parts: two vertex operators,  $\mathcal{V}_{L,R}(x) = e^{\frac{i}{\sqrt{2\pi K}} \gamma_{L,R} \tilde{\varphi}_{L,R}(x)}$ , that excite low-energy modes  $\tilde{\varphi}_{L,R}(x, t) = \tilde{\varphi}_{L,R}(x \pm vt)$  propagating with velocity  $\pm v$  and a free particle  $\tilde{d}^\dagger$  with velocity  $u$ , as schematically depicted in Fig. 1(b). The fractional charges of the three propagating parts can be measured with the charge density operator, which after rotation using Eq. (12) is given by

$$Q = \sqrt{\frac{K}{2\pi}} \partial_x (\tilde{\varphi}_L - \tilde{\varphi}_R) + \left( 1 - \frac{\gamma_R + \gamma_L}{2\pi} \right) \tilde{d}^\dagger \tilde{d}. \quad (14)$$

By calculating the commutator using Eq. (8), we have

$$[Q(y), \mathcal{V}_{R,L}(x)] = \frac{\gamma_{R,L}}{2\pi} \mathcal{V}_{R,L}(x) \delta(x - y). \quad (15)$$

Thus, the right- and left-moving vertex operators carry fractional charges  $n_{R,L} = \frac{\gamma_{R,L}}{2\pi}$  propagating with velocity  $\pm v$ . The remaining charge corresponding to the particle  $\tilde{d}^\dagger$  is  $n_I = 1 - n_R - n_L$  with velocity  $u$ .

In the tDMRG simulation, we use the Gaussian wave packet defined in Eq. (2); see Fig. 1(a). The propagation at half-filling,  $k_F = \pi/2$ , is shown in Fig. 2(a). Note that all parameters are known in this case:  $K = \frac{\pi}{2[\pi - \arccos(V)]}$ ,  $v = \frac{\pi \sqrt{1-V^2}}{2 \arccos(V)} = u / \sin(k_0)$ , and *momentum-independent* phase shifts  $\gamma_{R,L} = \pi(1 - K)$  [27]. In all cases, we observe three fractional humps that move with the exact velocities and magnitudes predicted by the nLL theory. Remarkably, the shape of the low-energy wave packets is stable over the whole energy regime, showing coherence over long times as it can be seen in Fig. 2(a). In addition, the variance of the high-energy hump,  $\sigma_h^2$ , grows in time according to Eq. (5) with an interaction-dependent effective mass; see Fig. 2(b). Therefore, the theoretical ad-hoc prediction of exactly three parts in the mode expansion (6) surprisingly provides a robust prediction of a free stable fractional particle. See the SM [52] for more details on the fitting procedure.

Here, spatial oscillations in the density with wave number  $2k_F$  have been averaged out by taking the average  $\rho_j(t)$  between two nearest-neighbor sites. They can be attributed to the staggered part of the density operator as discussed in the SM [52].

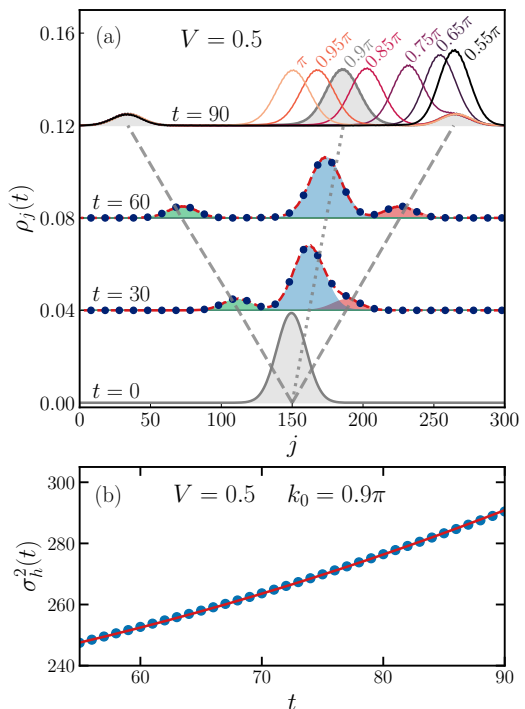


FIG. 2. Wave packet at half filling. (a) Snapshots of the averaged density profile for different times and  $V = 0.5$ . The time evolution is shown for  $k_0 = 0.9\pi$ . The gray dashed lines denote the light cone set by the velocity of the low-energy modes. The dotted line indicates the velocity of the high-energy particle. The shaded regions for the data  $t = 30$  and  $60$  show the time-dependent Gaussian functions which reproduce the tDMRG results represented by the symbols. The red dashed lines are the sums of the Gaussian functions. For  $t = 90$ , we show density profiles for the values of  $k_0$  indicated in the plot. (b) Variance of the high-energy hump vs.  $t$ . The red solid line is a fit to our estimates using a quadratic function [52].

In our analysis, we have used a large set of different values of  $t$ ,  $V$ , and  $k_0$ , which all show excellent agreement with the nLL theory. This implies that the nLL theory remarkably describes the *whole* energy regime covered by the Gaussian excitation with momentum  $k_0 > k_F$ . As predicted, we have not seen any momentum dependence in  $n_{R,L}$  [52]. Moreover, we observe a left-right symmetry in the low-energy humps, which is surprising since the initial wave packet at finite  $k_0$  clearly does not have this symmetry. Last but not least, we can apply the theory also to excitations very close to the Fermi energy, i.e.  $k_0 \rightarrow \pi/2$ . Once  $u \rightarrow v$ , longer and longer times  $t \gtrsim \tau_{\text{sp}} \equiv \sigma_0 / |v - u|$  are required to distinguish the two right-moving humps. In fact, this is in perfect agreement with conventional LL theory [6] of only one left- and one right-moving fractional charge with  $\frac{1-K}{2}$  and  $\frac{1+K}{2}$ , respectively [6]. Hence, the continuous crossover from nLL to LL behavior becomes very intuitive in the dynamics of fractional charges  $\frac{\gamma_{L,R}}{2\pi}$ . In contrast, this crossover is

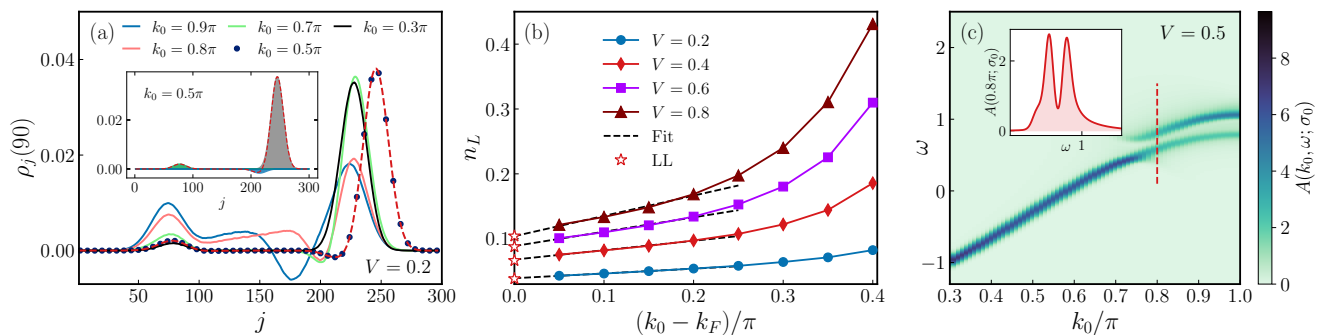


FIG. 3. Wave packet at quarter filling. (a) Averaged density profile for at fixed time  $t = 90$ ,  $V = 0.2$ , and distinct values of  $k_0$ . For  $k_0 = 0.5\pi$ , the symbols are the tDMRG results and the dashed line is the fit to our data considering the sum of three Gaussian functions, which are shown in the inset. (b) Charge of the left-moving hump as a function of momentum for different values of  $V$ . The dashed lines represent a linear fit of the data for  $(k_0 - k_F)/\pi \leq 0.2$ . The stars on the vertical axis mark the LL prediction  $(1 - K)/2$ , valid for  $k_0 \rightarrow k_F$ . (c) Spectral function  $A(k_0, \omega; \sigma_0)$ , see Eq. (16), calculated for  $V = 0.5$ . The inset shows a cut for momentum  $k_0 = 0.8\pi$ . The peak at higher frequencies is a signature of bound states.

much more involved in the frequency domain since the threshold exponents are quadratic functions of the phase shifts [26].

*Quarter filling.*—To illustrate a more generic situation, we now consider the model in Eq. (1) at quarter filling,  $k_F = \pi/4$ . In this case, by solving Bethe ansatz equations, we can numerically determine the exact renormalized dispersion, Luttinger parameter, and velocity of the low-energy modes [1, 50].

Figure 3(a) shows tDMRG results for  $V = 0.2$  and different values of  $k_0$  at  $t = 90$  after averaging the density over four neighboring sites to smooth the  $2k_F$  oscillations out. In the low-energy regime, e.g. for  $k_0 = 0.3\pi$ , we observe only one left and one right hump moving with velocities  $\pm v$ , similar to the half-filled case. However, now the charge  $n_L$  carried by the left-moving hump varies with  $k_0$  as shown in Fig. 3(b), which in turn directly provides the momentum-dependent phase shifts  $\gamma_L = 2\pi n_L$ . In the extrapolation  $k_0 \rightarrow k_F$  we recover the LL prediction  $n_L \rightarrow \frac{1-K}{2}$ .

For larger values of  $k_0$ , see for example  $k_0 = 0.5\pi$  and  $0.7\pi$  in Fig. 3(a), the three signals predicted by the nLL are observed again: two counter-propagating charges  $n_{R,L} = \frac{\kappa_{R,L}}{2\pi(v \mp u)}$  moving with velocities  $\pm v$ , and a large right-moving hump with velocity  $u$ . Note that the right low-energy mover carries *negative* charge since  $u > v$ . We again find that the time evolution of the excitation can be predicted by three propagating Gaussian wave packets [52].

As we increase the momentum, the density profile develops a complex pattern. For  $k_0 = 0.8\pi$  in Fig. 3(a), the broad feature around the middle of the chain suggests the presence of additional excitations. In fact, the operator in Eq. (2) can create not only individual particles but also composite excitations with net charge  $+1$ . To analyze the excitations, we consider the Fourier transform of the overlap between the initial state in Eq. (2) and the

time-evolved one

$$A(k_0, \omega; \sigma_0) = \int_{-\infty}^{\infty} dt e^{i(\omega - E_0)t} \langle \Psi(0) | \Psi(t) \rangle, \\ = 2\pi \sum_{\alpha} |\langle \alpha | \Psi(0) \rangle|^2 \delta(\omega - E_{\alpha} + E_0), \quad (16)$$

where  $|\alpha\rangle$  are eigenstates of  $H$  with energy  $E_{\alpha}$  above the ground-state energy  $E_0$ . In the limit  $\sigma_0 \rightarrow \infty$ , it reduces to the standard single-particle spectral function [55]. We compute  $A(k_0, \omega; \sigma_0)$  by performing a fast Fourier transform with a cosine window in the interval  $t \in [-t_{\max}, t_{\max}]$ , with  $t_{\max} = 90$ .

As discussed in Ref. [55], the nLL theory for  $A(k_0, \omega, \sigma_0 \rightarrow \infty)$  predicts a diverging peak at the dispersion  $\omega = \varepsilon_p$ , which decays as power laws on both sides with exponents dependent on the phase shifts. In our results of  $A(k_0, \omega; \sigma_0)$ , this is reflected as a broad single-particle peak for  $k_0 \lesssim 0.6\pi$ ; see Fig. 3(c). At larger momenta,  $A(k_0, \omega; \sigma_0)$  displays a double-peak structure for  $k_0$  near  $\pi$ , which is a clear indication of a yet unaccounted excitation in the wave packet  $|\Psi(0)\rangle$  in Eq. (?). This feature is absent for half-filling [52].

We identify this excitation as a composite of a two-particle bound state with a free hole as depicted in Fig. 1(c), which has been predicted in Ref. [55]. Such a composite gives a high-energy continuum in the spectral function for momenta greater than  $\pi + k_F - Q_{\text{bs}}$ , where  $Q_{\text{bs}} = [\pi - 2\arccos(V)](1 - \frac{2k_F}{\pi})$  restricts the momentum of bound state  $|\pi - k_{\text{bs}}| < Q_{\text{bs}}$ . Note that  $Q_{\text{bs}}$  vanishes for  $V \rightarrow 0$  or  $k_F \rightarrow \frac{\pi}{2}$ . In nLL theory, this type of excitation can be described by  $c_j^{\dagger} \sim e^{-ik_0 x} B^{\dagger}(x) h^{\dagger}(x)$  [55]. For  $k_0 = 0.8\pi$  in Fig. 3(a), both the bound state ( $B^{\dagger}$ ) and the hole ( $h^{\dagger}$ ) are created near the bottom of their respective bands. This implies a low velocity, consistent with a slow-moving hump. In general, the evolution of the wave packet may involve contributions from low- or high-energy particles, holes, and bound states

that share the total momentum covered by the Gaussian distribution; see the SM [52].

*Conclusions.*— We proposed an out-of-equilibrium protocol to investigate the fractionalization of high-energy excitations in critical chains. We clarified the crossover between LL and nLL regimes and identified contributions from elementary particles moving with different velocities and carrying fractional charges, which can be negative for  $u > v$ . The transport simulations reveal also more involved excitations, such composite excitations formed by holes and bound states. This analysis also applies to quantum spin chains and spin-charge separated quantum fluids [56, 57]. Our work paves the way for precision tests of nLL effects through non-equilibrium dynamics in ultracold-atom platforms [58, 59] and time-resolved measurements of hot electrons in quantum wires and quantum Hall edge states [60–62]. In particular, we find a fractionally charged particle with free-particle dynamics, a right-moving low-energy excitation which can be negatively charged, and a left-moving signal that gives an exact measurement of the interaction couplings in a large parameter regime. Hence, experimental measurements of counter-propagating fractional charges directly provide quantitative values of the momentum-dependent interactions in the linear and the nonlinear regimes.

This work was supported by the Deutsche Forschungsgemeinschaft (DFG, German Research Foundation) - Project No. 277625399-TRR 185 OSCAR (A4,A5), by the Conselho Nacional de Desenvolvimento Científico e Tecnológico (R.G.P.), and by a grant from the Simons Foundation (Grant No. 1023171, R.G.P.). The authors thank the high-performance cluster Elwetritsch for providing computational resources.

- 
- [1] T. Giamarchi, *Quantum physics in one dimension* (Clarendon Press, Oxford, 2004).
- [2] F. D. M. Haldane, ‘Luttinger liquid theory’ of one-dimensional quantum fluids. I. Properties of the Luttinger model and their extension to the general 1D interacting spinless Fermi gas, *J. Phys. C* **14**, 2585 (1981).
- [3] V. V. Deshpande, M. Bockrath, L. I. Glazman, and A. Yacoby, Electron liquids and solids in one dimension, *Nature* **464**, 209 (2010).
- [4] S. Tomonaga, Remarks on Bloch’s Method of Sound Waves applied to Many-Fermion Problems, *Prog. Theor. Phys.* **5**, 544 (1950).
- [5] J. M. Luttinger, An Exactly Soluble Model of a Many-Fermion System, *J. Math. Phys.* **4**, 1154 (1963).
- [6] K.-V. Pham, M. Gabay, and P. Lederer, Fractional excitations in the Luttinger liquid, *Phys. Rev. B* **61**, 16397 (2000).
- [7] J. M. Leinaas, M. Horsdal, and T. H. Hansson, Sharp fractional charges in Luttinger liquids, *Phys. Rev. B* **80**, 115327 (2009).
- [8] H. Steinberg, G. Barak, A. Yacoby, L. N. Pfeiffer, K. W. West, B. I. Halperin, and K. L. Hur, Charge fractionalization in quantum wires, *Nat. Phys.* **4**, 116 (2007).
- [9] K. Le Hur, B. I. Halperin, and A. Yacoby, Charge fractionalization in nonchiral Luttinger systems, *Ann. Phys. (N. Y.)* **323**, 3037 (2008).
- [10] H. Kamata, N. Kumada, M. Hashisaka, K. Muraki, and T. Fujisawa, Fractionalized wave packets from an artificial Tomonaga–Luttinger liquid, *Nat. Nanotechnol.* **9**, 177 (2014).
- [11] V. Freulon, A. Marguerite, J. M. Berroir, B. Plaças, A. Cavanna, Y. Jin, and G. Fève, Hong-Ou-Mandel experiment for temporal investigation of single-electron fractionalization, *Nat. Commun.* **6**, 6854 (2015).
- [12] C. Kim, A. Y. Matsuura, Z.-X. Shen, N. Motoyama, H. Eisaki, S. Uchida, T. Tohyama, and S. Maekawa, Observation of Spin-Charge Separation in One-Dimensional SrCuO<sub>2</sub>, *Phys. Rev. Lett.* **77**, 4054 (1996).
- [13] P. Segovia, D. Purdie, M. Hengsberger, and Y. Baer, Observation of spin and charge collective modes in one-dimensional metallic chains, *Nature* **402**, 504 (1999).
- [14] O. M. Auslaender, A. Yacoby, R. de Picciotto, K. W. Baldwin, L. N. Pfeiffer, and K. W. West, Tunneling Spectroscopy of the Elementary Excitations in a One-Dimensional Wire, *Science* **295**, 825 (2002).
- [15] O. M. Auslaender, H. Steinberg, A. Yacoby, Y. Tserkovnyak, B. I. Halperin, K. W. Baldwin, L. N. Pfeiffer, and K. W. West, Spin-Charge Separation and Localization in One Dimension, *Science* **308**, 88 (2005).
- [16] B. J. Kim, H. Koh, E. Rotenberg, S.-J. Oh, H. Eisaki, N. Motoyama, S. Uchida, T. Tohyama, S. Maekawa, Z.-X. Shen, and C. Kim, Distinct spinon and holon dispersions in photoemission spectral functions from one-dimensional SrCuO<sub>2</sub>, *Nat. Phys.* **2**, 397 (2006).
- [17] M. Mourigal, M. Enderle, A. Klöpperpieper, J.-S. Caux, A. Stunault, and H. M. Rønnow, Fractional spinon excitations in the quantum Heisenberg antiferromagnetic chain, *Nat. Phys.* **9**, 435 (2013).
- [18] T. Kinoshita, T. Wenger, and D. S. Weiss, Observation of a One-Dimensional Tonks-Girardeau Gas, *Science* **305**, 1125 (2004).
- [19] B. Paredes, A. Widera, V. Murg, O. Mandel, S. Fölling, I. Cirac, G. V. Shlyapnikov, T. W. Hänsch, and I. Bloch, Tonks-Girardeau gas of ultracold atoms in an optical lattice, *Nature* **429**, 277 (2004).
- [20] G. Pagano, M. Mancini, G. Cappellini, P. Lombardi, F. Schäfer, H. Hu, X.-J. Liu, J. Catani, C. Sias, M. Inguscio, and L. Fallani, A one-dimensional liquid of fermions with tunable spin, *Nat. Phys.* **10**, 198 (2014).
- [21] T. A. Hilker, G. Salomon, F. Grusdt, A. Omran, M. Boll, E. Demler, I. Bloch, and C. Gross, Revealing hidden antiferromagnetic correlations in doped Hubbard chains via string correlators, *Science* **357**, 484 (2017).
- [22] A. Imambekov, T. L. Schmidt, and L. I. Glazman, One-dimensional quantum liquids: Beyond the Luttinger liquid paradigm, *Rev. Mod. Phys.* **84**, 1253 (2012).
- [23] A. V. Rozhkov, Fermionic quasiparticle representation of Tomonaga-Luttinger Hamiltonian, *Eur. Phys. J. B* **47**, 193 (2005).
- [24] M. Pustilnik, M. Khodas, A. Kamenev, and L. I. Glazman, Dynamic Response of One-Dimensional Interacting Fermions, *Phys. Rev. Lett.* **96**, 196405 (2006).
- [25] M. Khodas, M. Pustilnik, A. Kamenev, and L. I. Glazman, Fermi-Luttinger liquid: Spectral function of interacting one-dimensional fermions, *Phys. Rev. B* **76**,

- 155402 (2007).
- [26] A. Imambekov and L. I. Glazman, Universal Theory of Nonlinear Luttinger Liquids, *Science* **323**, 228 (2009).
- [27] R. G. Pereira, S. R. White, and I. Affleck, Exact Edge Singularities and Dynamical Correlations in Spin-1/2 Chains, *Phys. Rev. Lett.* **100**, 027206 (2008).
- [28] V. V. Cheianov and M. Pustilnik, Threshold Singularities in the Dynamic Response of Gapless Integrable Models, *Phys. Rev. Lett.* **100**, 126403 (2008).
- [29] A. Imambekov and L. I. Glazman, Exact Exponents of Edge Singularities in Dynamic Correlation Functions of 1D Bose Gas, *Phys. Rev. Lett.* **100**, 206805 (2008).
- [30] F. H. L. Essler, Threshold singularities in the one-dimensional Hubbard model, *Phys. Rev. B* **81**, 205120 (2010).
- [31] R. G. Pereira, Long time correlations of nonlinear Luttinger liquids, *Int. J. Mod. Phys. B* **26**, 1244008 (2012).
- [32] E. Bettelheim, A. G. Abanov, and P. Wiegmann, Orthogonality Catastrophe and Shock Waves in a Nonequilibrium Fermi Gas, *Phys. Rev. Lett.* **97**, 246402 (2006).
- [33] E. Bettelheim and L. Glazman, Quantum Ripples Over a Semiclassical Shock, *Phys. Rev. Lett.* **109**, 260602 (2012).
- [34] I. V. Protopopov, D. B. Gutman, P. Schmitteckert, and A. D. Mirlin, Dynamics of waves in one-dimensional electron systems: Density oscillations driven by population inversion, *Phys. Rev. B* **87**, 045112 (2013).
- [35] I. V. Protopopov, D. B. Gutman, M. Oldenburg, and A. D. Mirlin, Dissipationless kinetics of one-dimensional interacting fermions, *Phys. Rev. B* **89**, 161104 (2014).
- [36] G. Barak, H. Steinberg, L. N. Pfeiffer, K. W. West, L. Glazman, F. von Oppen, and A. Yacoby, Interacting electrons in one dimension beyond the Luttinger-liquid limit, *Nat. Phys.* **6**, 489 (2010).
- [37] Y. Jin, O. Tsyplatyev, M. Moreno, A. Anthore, W. K. Tan, J. P. Griffiths, I. Farrer, D. A. Ritchie, L. I. Glazman, A. J. Schofield, and C. J. B. Ford, Momentum-dependent power law measured in an interacting quantum wire beyond the Luttinger limit, *Nat. Commun.* **10** (2019).
- [38] S. Wang, S. Zhao, Z. Shi, F. Wu, Z. Zhao, L. Jiang, K. Watanabe, T. Taniguchi, A. Zettl, C. Zhou, and F. Wang, Nonlinear Luttinger liquid plasmons in semiconducting single-walled carbon nanotubes, *Nat. Mater.* **19**, 986 (2020).
- [39] R. Senaratne, D. Cavazos-Cavazos, S. Wang, F. He, Y.-T. Chang, A. Kafle, H. Pu, X.-W. Guan, and R. G. Hulet, Spin-charge separation in a one-dimensional Fermi gas with tunable interactions, *Science* **376**, 1305 (2022).
- [40] S. R. White and A. E. Feiguin, Real-Time Evolution Using the Density Matrix Renormalization Group, *Phys. Rev. Lett.* **93**, 076401 (2004).
- [41] E. A. Jagla, K. Hallberg, and C. A. Balseiro, Numerical study of charge and spin separation in low-dimensional systems, *Phys. Rev. B* **47**, 5849 (1993).
- [42] B. Trauzettel, I. Safi, F. Dolcini, and H. Grabert, Appearance of fractional charge in the noise of nonchiral Luttinger liquids, *Phys. Rev. Lett.* **92**, 226405 (2004).
- [43] C. Kollath, U. Schollwöck, and W. Zwerger, Spin-Charge Separation in Cold Fermi Gases: A Real Time Analysis, *Phys. Rev. Lett.* **95**, 176401 (2005).
- [44] T. Ulbricht and P. Schmitteckert, Is spin-charge separation observable in a transport experiment? *EPL* **86**, 57006 (2009).
- [45] K. A. Al-Hassanieh, J. Rincón, E. Dagotto, and G. Alvarez, Wave-packet dynamics in the one-dimensional extended Hubbard model, *Phys. Rev. B* **88**, 045107 (2013).
- [46] M. Acciai, A. Calzona, G. Dolcetto, T. L. Schmidt, and M. Sasseti, Charge and energy fractionalization mechanism in one-dimensional channels, *Phys. Rev. B* **96**, 075144 (2017).
- [47] S. Scoppa, P. Calabrese, and L. Piroli, Real-time spin-charge separation in one-dimensional Fermi gases from generalized hydrodynamics, *Phys. Rev. B* **104**, 115423 (2021).
- [48] A. Moreno, A. Muramatsu, and J. M. P. Carmelo, Charge and spin fractionalization beyond the Luttinger-liquid paradigm, *Phys. Rev. B* **87**, 075101 (2013).
- [49] A. A. Dontsov and A. P. Dmitriev, Charge fractionalization beyond the Luttinger liquid paradigm: An analytical consideration, *Phys. Rev. B* **103**, 195148 (2021).
- [50] V. E. Korepin, N. M. Bogoliubov, and A. G. Izergin, *Quantum Inverse Scattering Method and Correlation Functions* (Cambridge University Press, 1993).
- [51] R. Shankar, *Principles of Quantum Mechanics* (Springer, 1994).
- [52] See the Supplemental Material for a detailed analysis of the free fermion wave packet, the spectral function at half filling, and the momentum-dependent charge of the left-moving hump at quarter filling.
- [53] Y. Tsukamoto, T. Fujii, and N. Kawakami, Critical behavior of Tomonaga-Luttinger liquids with a mobile impurity, *Phys. Rev. B* **58**, 3633 (1998).
- [54] L. Balents, X-ray-edge singularities in nanotubes and quantum wires with multiple subbands, *Phys. Rev. B* **61**, 4429 (2000).
- [55] R. G. Pereira, S. R. White, and I. Affleck, Spectral function of spinless fermions on a one-dimensional lattice, *Phys. Rev. B* **79**, 165113 (2009).
- [56] T. L. Schmidt, A. Imambekov, and L. I. Glazman, Fate of 1D Spin-Charge Separation Away from Fermi Points, *Phys. Rev. Lett.* **104**, 116403 (2010).
- [57] F. H. L. Essler, R. G. Pereira, and I. Schneider, Spin-charge-separated quasiparticles in one-dimensional quantum fluids, *Phys. Rev. B* **91**, 245150 (2015).
- [58] P. L. Pedersen, M. Gajdacz, N. Winter, A. J. Hilliard, J. F. Sherson, and J. Arlt, Production and manipulation of wave packets from ultracold atoms in an optical lattice, *Phys. Rev. A* **88**, 023620 (2013).
- [59] J. Vijayan, P. Sompet, G. Salomon, J. Koepsell, S. Hirthe, A. Bohrdt, F. Grusdt, I. Bloch, and C. Gross, Time-resolved observation of spin-charge deconfinement in fermionic Hubbard chains, *Science* **367**, 186 (2020).
- [60] M. Kataoka, N. Johnson, C. Emary, P. See, J. P. Griffiths, G. A. C. Jones, I. Farrer, D. A. Ritchie, M. Pepper, and T. J. B. M. Janssen, Time-of-Flight Measurements of Single-Electron Wave Packets in Quantum Hall Edge States, *Phys. Rev. Lett.* **116**, 126803 (2016).
- [61] M. Hashisaka, N. Hiyama, T. Akiho, K. Muraki, and T. Fujisawa, Waveform measurement of charge- and spin-density wavepackets in a chiral Tomonaga-Luttinger liquid, *Nat. Phys.* **13**, 559 (2017).
- [62] C. Bäuerle, D. C. Glatzli, T. Meunier, F. Portier, P. Roche, P. Roulleau, S. Takada, and X. Waintal, Coherent control of single electrons: a review of current progress, *Rep. Prog. Phys.* **81**, 056503 (2018).

## SUPPLEMENTAL MATERIAL

### Free-fermion case

We use the exact solution of the free-fermion case to benchmark our tDMRG results. In Fig. 4, we show snapshots of typical density profiles for half filling. We find an excellent agreement between the analytical formula and the numerical simulation. Due to the relatively small variance in the Fourier space, all the one-particle states with significant probability amplitude have roughly the same velocity. As a consequence, we observe the coherent motion of the wave packet.

### Oscillations in the density profile

The numerical results reveal that in the interacting case the density profile develops oscillations as soon as the counter-propagating humps start to split. This effect can be observed for the low- and high-energy regimes in Fig 5(a) and (b), respectively. To separate the alternating part from the smooth one, we evaluate the absolute value of the difference between the local charge excess in neighboring sites, defining

$$\Delta\rho_j(t) = \frac{1}{2}|\rho_j(t) - \rho_{j+1}(t)|. \quad (17)$$

The result for  $\Delta\rho_j(t)$  is represented by the black lines in Fig. 5(b). The wave front of the alternating part moves along the smooth part of the fastest density humps, but the alternating part has a long tail that persists after the smooth part has propagated away. We stress that the alternating part does not contribute to the net charge being transported away from the region where the excitation was initially created.

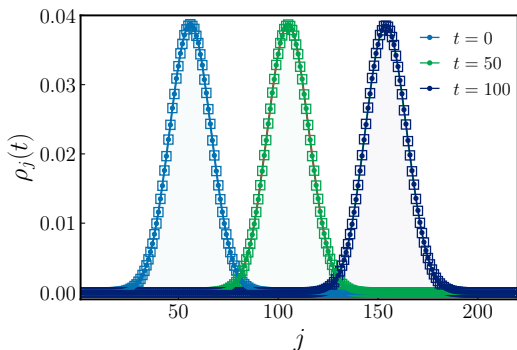


FIG. 4. Snapshots of the density profile for  $k_0 = 0.56\pi$  and half filling in the noninteracting model,  $V = 0$ . The filled circles are the exact results obtained via Eq. (4) of the main text and the squares are tDMRG data. The results were obtained setting  $L = 220$ ,  $\sigma_0 = 14.5$ , and  $j_0 = 55$ .

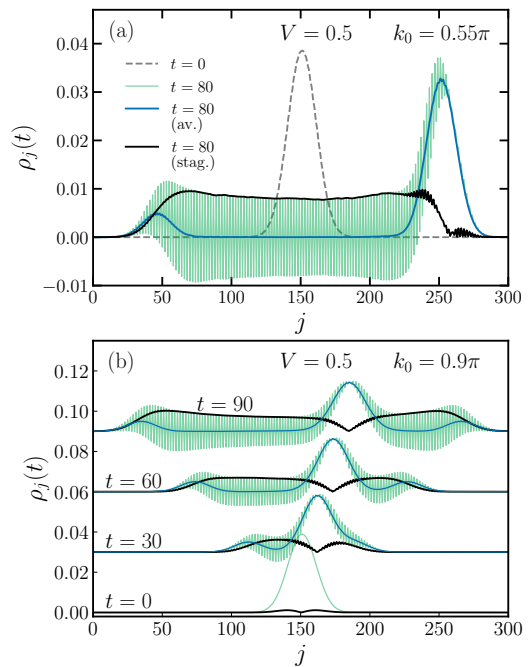


FIG. 5. Snapshots of the density profile for (a)  $k_0 = 0.55\pi$  and (b)  $k_0 = 0.9\pi$ , half filling and  $V = 0.5$ . The green and blue lines represent the local charge excess before and after the two-site average, respectively. The black lines represent the two-site difference  $\Delta\rho_j(t)$ , see Eq. (17), which selects the alternating part of the density profile.

We can use the effective field theory to understand how the oscillations arise only in the presence of interactions. The bosonized form of the density operator is [1]

$$n_j \sim \sqrt{\frac{K}{2\pi}}(\partial_x\varphi_L - \partial_x\varphi_R) + \frac{1}{2\pi\alpha} \cos\left[\sqrt{2\pi K}(\varphi_L - \varphi_R) - 2k_F x\right], \quad (18)$$

where  $\alpha$  is a nonuniversal short-distance cutoff of the order of the lattice spacing. The second term is the staggered part that oscillates with momentum  $2k_F$ .

At low energies, we take  $k_0 \rightarrow k_F$  and  $c_j^\dagger \rightarrow e^{-ik_F x}\psi_R^\dagger(x) + e^{ik_F x}\psi_L^\dagger(x)$  in Eq. (2). Setting  $j_0 = 0$  in an infinite chain, the expectation value of the staggered part in the time-evolved state becomes

$$\rho_j^{\text{st}}(t) = \frac{A^2 e^{-i2k_F x}}{4\pi\alpha} \int dx' dx'' e^{-\frac{(x')^2}{2\sigma_0^2}} e^{-\frac{(x'')^2}{2\sigma_0^2}} e^{-i2k_F x'} \times \langle \psi_L(x') e^{i\sqrt{2\pi K}[\varphi_L(x,t) - \varphi_R(x,t)]} \psi_R^\dagger(x'') \rangle + \text{c.c.} \quad (19)$$

Bosonizing the fermion operators, we obtain

$$\begin{aligned} \rho_j^{\text{st}}(t) &\sim e^{-i2k_F x} \int dx' dx'' e^{-\frac{(x')^2}{2\sigma_0^2}} e^{-\frac{(x'')^2}{2\sigma_0^2}} e^{-i2k_F x'} \\ &\quad \times \langle \mathcal{V}_R(x'; K - \nu) \mathcal{V}_R(x - vt; -K) \mathcal{V}_R(x''; \nu) \rangle \\ &\quad \times \langle \mathcal{V}_L(x'; -\nu) \mathcal{V}_L(x + vt; K) \mathcal{V}_L(x''; \nu - K) \rangle \\ &\quad + \text{c.c.} \end{aligned} \quad (20)$$

$$\begin{aligned} \rho_j^{\text{st}}(t) &\sim e^{-i2k_F x} \int_{-\infty}^{\infty} dx'' e^{-\frac{(x'')^2}{2\sigma_0^2}} (x - vt - x'' + i\alpha)^{-\frac{1+K}{2}} (x + vt - x'' - i\alpha)^{\frac{1-K}{2}} \\ &\quad \times \int_{-\infty}^{\infty} dx' e^{-i2k_F x'} e^{-\frac{(x')^2}{2\sigma_0^2}} (x' - x + vt + i\alpha)^{\frac{1-K}{2}} [(x' - x'')^2 + \alpha^2]^{-\frac{1-K^2}{4K}} (x' - x - vt - i\alpha)^{-\frac{1+K}{2}} + \text{c.c.} \end{aligned} \quad (22)$$

From Eq. (22) we can check that there are no oscillations in the noninteracting case. Setting  $K = 1$  for  $V = 0$ , the result simplifies to

$$\begin{aligned} \rho_j^{\text{st}}(t) &\sim e^{-i2k_F x} \int_{-\infty}^{\infty} dx'' e^{-\frac{(x'')^2}{2\sigma_0^2}} (x - vt - x'' + i\alpha)^{-1} \\ &\quad \times \int_{-\infty}^{\infty} dx' e^{-i2k_F x'} e^{-\frac{(x')^2}{2\sigma_0^2}} (x' - x - vt - i\alpha)^{-1} \\ &\quad + \text{c.c.} \end{aligned} \quad (23)$$

The integral over  $x'$  vanishes because the integrand is an analytical function in the lower half plane. For  $K \neq 1$ , the integrand in Eq. (22) has branch cuts both above and below the real axis and the staggered part of the density operator acquires a nonzero expectation value. Physically, the branch points at  $x' = x \pm vt$  are associated with excitations moving in opposite directions.

### Momentum independence at half filling

To avoid the reflection of the wave packet at the boundaries, the time reached in the tDMRG simulations is fixed by system size and the interaction. This limitation on the maximum time may prevent distinguishing the two right-moving humps. In Fig. 6, we show the charges  $n_{R,L}$  as a function of the LL parameter for two distinct values of  $k_0$ . In these cases, both right and left low-energy movers can be separately resolved and we observe an excellent agreement with the nLL prediction,  $n_{R,L} = (1 - K)/2$ .

Now, for the cases in which we cannot resolve the right-moving excitations, we analyze the dynamics by assuming that the density profile consists of two symmetric counter-propagating humps with velocity  $v$  and a middle one with mean velocity  $u = v \sin(k_0)$ . We fit our results using the following equation

where  $\nu = \frac{1+K}{2}$ . The three-point function for the chiral vertex operators has the form

$$\begin{aligned} &\langle \mathcal{V}_{R,L}(x_1; n_1) \mathcal{V}_{R,L}(x_2; n_2) \mathcal{V}_{R,L}(x_3; n_3) \rangle \\ &= \prod_{i < j} (x_i - x_j \pm i\alpha)^{n_i n_j / K}, \end{aligned} \quad (21)$$

provided that the neutrality condition  $\sum_i n_i = 0$  is satisfied. We then have

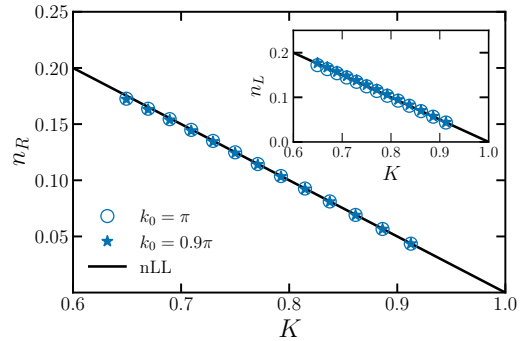


FIG. 6. Charge carried by the right movers for  $k_0 = 0.9\pi$  and  $\pi$ . The charge of the left movers is shown in the inset. The solid lines are the nLL predictions,  $n_{R,L} = (1 - K)/2$

$$\rho_j(t) = A \left[ e^{-\frac{(j-j_0-vt)^2}{\sigma_l^2}} + e^{-\frac{(j-j_0+vt)^2}{\sigma_l^2}} \right] + \tilde{A} e^{-\frac{(j-j_0-ut)^2}{\sigma_h^2}}, \quad (24)$$

where the amplitude  $A$  and the variance  $\sigma_l$  are obtained by fitting the left-moving wave packet. The amplitude  $\tilde{A}$  and the variance of the high-energy wave packet are fitting parameters. In Fig. 7(a), we show combinations of three Gaussian functions that describe the time evolution of the charge wave packet. For  $V = 0.5$  and  $k_0 = 0.8\pi$ , the fixed parameters of the low-energy contributions are  $\sigma_l = 14.74$  and  $A = 0.0048$ . The free fitting parameters  $\tilde{A}$  and  $\sigma_h$  depend on time and vary monotonically once the left movers can be discerned from the right-moving excitation; see Fig. 7(b).

As aforementioned, in the free-fermion case, a Gaussian wave packet of a single particle that is strongly peaked around  $k_0$  spreads in time as  $\sigma^2(t) \approx \sigma_0^2(1 + \frac{t^2}{m_0^2 \sigma_0^4})$ . In this context, by fitting our estimates of  $\sigma_h^2(t)$



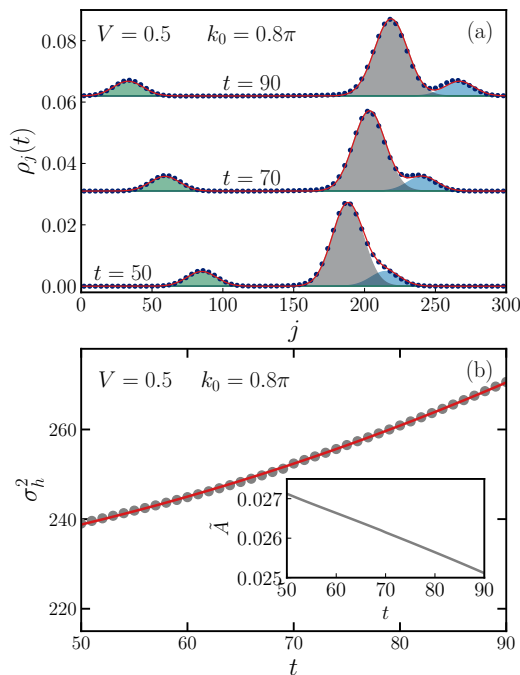


FIG. 7. (a) Snapshots of the averaged density profile for  $V = 0.5$ ,  $k_0 = 0.8\pi$  and  $t = 50, 70$ , and  $90$ . The symbols are tDMRG results and the red lines fit our data considering Eq. (24). The shaded regions represent the three Gaussian functions that are combined to produce the density profile. (b) Time dependence of the fitting parameters  $\sigma_l$  and  $\tilde{A}$  (see the inset). The red line is the fit to our data using  $\sigma_h^2(t) = a + bt^2$ .

considering the function  $\sigma_h^2(t) = a + bt^2$ , we obtain  $b = 0.006$ . Overall, we find that the combination of three Gaussian functions is consistent with our DMRG results.

### Spectral decomposition of the initial excitation

In the main text, we discuss the spectral decomposition of the initial excitation for quarter filling. In addition to the signature of one-particle states, we observe the emergence of two-particle bound states, which do not exist for the half-filling case [55]. Indeed, the function  $A(k_0, \omega; \sigma_0)$  is characterized by a single peak in the vicinity of the high-energy particle excitations (see Fig. 8).

### Wave-packet dynamics at quarter filling

In contrast to the half-filling case, where one-particle states dominate the time evolution of the Gaussian excitation, additional high-energy states play an important role at low densities. In this case, we observe that the dynamics may harbor two-particle bound states and free holes, whose fingerprint is observed in  $A(k_0, \omega; \sigma_0)$ . As

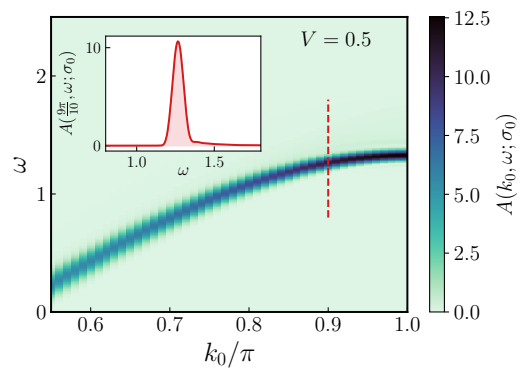


FIG. 8. Function  $A(k_0, \omega; \sigma)$  for  $V = 0.5$ . The dominance of the high-energy particle excitations is unveiled by the single-peak pattern around  $\varepsilon(k_0) = -v \cos(k_0)$ . The inset shows a cut for  $k_0 = \frac{9\pi}{10}$ .

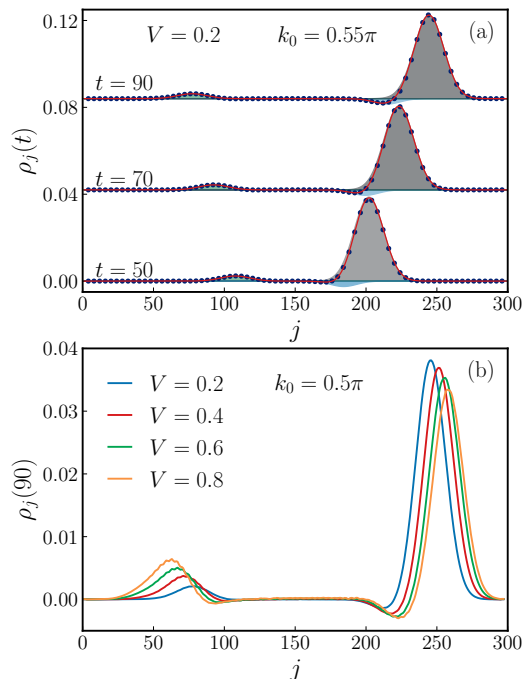


FIG. 9. (a) Averaged density profile for  $k_0 = \pi/2$ ,  $t = 90$  and distinct values of  $V$ . (b) Snapshots of the averaged density profile for  $V = 0.2$  and  $k_0 = 0.55\pi$ . The time evolution of the wave packet can be described by the propagation of three Gaussian functions represented by the shaded regions on the plot, whose sum produces the red solid lines. The symbols are the DMRG results.

discussed in the main text, the minimum value of momentum for which the aforementioned composite excitation exists is

$$k \geq \pi + k_F - Q_{\text{bs}}. \quad (25)$$

with  $Q_{\text{bs}} = [\pi - 2 \arccos(V)] (1 - \frac{2k_F}{\pi})$ . Thus, to observe the nLL prediction discussed in the main text, we must set appropriate values of  $k_0$  and  $V$  such that *only* single-

particle excitations are created in the initial state. For instance, for  $V = 0.2$  and  $k_0 \lesssim 0.7\pi$ , we observe that the late-time excitation comprises a three-hump structure, as predicted by nLL. In this regime, we can describe the evolution of the initial excitation using a combination of three propagating Gaussian wave packets. In Fig. 9(a), we show snapshots of the averaged density profile for  $V = 0.2$  and  $k_0 = 0.55\pi$ . The decomposition of the excitation into three Gaussian functions is represented by the shaded regions in the figure. The velocities  $v = 0.764$  and  $u = 1.06$  are the obtained via Bethe ansatz. Note that the right-moving excitation is composed by one Gaussian function with a *negative* amplitude that follows velocity  $v$  and one hump with ve-

locity of the high-energy particle with momentum  $k_0$ . It is worth pointing out that the negative charge carried by the low-energy right-moving hump is consistent with the nLL description,  $n_R \propto 1/(v - u) < 0$ . In general, we found a good agreement between the combination of three Gaussian functions and the tDMRG results as long as we do not have composite excitations in the dynamics.

Finally, let us briefly discuss a case where we see signatures of the bound states, but we can still discern the left- and right-propagating excitations; see Fig. 9(b). Depending on  $k_0$ , the left-moving wave packet is not only composed by low-energy movers, but a combination of excitations with velocity close to  $-v$ . Indeed, the tail of the left wave packet in Fig. 9(b) suggests the existence of holes propagating with velocity close to the Fermi one.